

On Criminal Identification in Color Skin Images Using Skin Marks (RPPVSM) and Fusion with Vein Patterns

Arfika Nurhudatiana*, *Student Member, IEEE* and Adams Wai-Kin Kong, *Member, IEEE*

Abstract—Relatively Permanent Pigmented or Vascular Skin Marks (RPPVSM) were recently introduced as a biometric trait for identification in evidence images showing only the non-facial skin of the criminals or victims, such as in the cases of child sexual abuse, masked gunmen, and riots. As manual RPPVSM identification is tiring and time consuming, an automated RPPVSM identification system comprising skin segmentation, RPPVSM detection, and RPPVSM matching algorithms is proposed in this paper. A fusion scheme integrating RPPVSM with vein patterns is also proposed to handle scenarios with limited RPPVSM, such as when only arm or thigh is visible from the evidence images. To evaluate the system and the fusion, two experiments were performed. The first experiment evaluated the proposed RPPVSM identification system on 1,200 images of backs collected from 283 Asian and Caucasian subjects in varying pose and viewpoint conditions and the second experiment evaluated the fusion of RPPVSM and vein patterns on 2,360 images of chests, forearms, and thighs collected from mostly Asian subjects. The results are encouraging. The proposed RPPVSM detection algorithm outperforms existing skin mark detection methods previously proposed for face biometrics and the fusion scheme with RPPVSM improves vein identification in all body parts. To the best of our knowledge, this is the first work on automated personal identification based on non-facial skin marks in forensic settings.

Index Terms—Forensics, biometrics, skin mark, vein, fusion, criminal identification

I. INTRODUCTION

NOWADAYS, it has become easier for anyone to produce digital images in day to day life. Along with this trend, digital images have become increasingly important in forensic investigations. Using these images for criminal and victim identification can be very challenging at times. One of the challenges is the lack of biometric traits available for identification. Gunmen, terrorists, and rioters often cover their faces with masks or clothing, making face recognition

impossible [1]-[5]. The same challenges are encountered in the cases of child sexual abuse (e.g., child pornography), where pedophiles' faces and tattoos are rarely visible in the evidence images or purposely blurred to avoid recognition. However, it is not rare to observe bare skin of other body parts, such as back, chest, arm, and thigh in the evidence images of these cases. For example, rioters and masked gunmen often wear short sleeve shirts revealing their bare hands and arms despite having their faces covered [1]-[3] and sometimes even take their shirts off and show their chests and backs [4], [5]. The image quality of rioters and protesters can be very high since news reporters use professional cameras to capture the images. The quality of child sexual abuse images is also usually high since the typical resolutions of commonly available digital cameras are higher than five megapixels. Moreover, in the scenario of self-taken child sexual abuse images, close-up views of pedophiles' and victims' naked bodies can often be seen due to the short distances between the cameras and the subjects.

Relatively Permanent Pigmented or Vascular Skin Marks (RPPVSM), which include but are not limited to nevi, lentigines (lentigos), cherry hemangiomas, and seborrheic keratoses, were recently proposed as a biometric trait [6], [7]. The concept of RPPVSM as a biometric trait was originated from the trials of the child sexual abuse case *United States v. Michael Joseph Pepe* (2008), where a nevi pattern located on the left thigh of a suspect was used to verify the criminal in the evidence images [8], [9]. RPPVSM are common in various races and stable over a long period of time (i.e., six months or longer) [10], [11]. Under certain conditions, patterns with seven or more RPPVSM are also highly distinctive [7]. Although skin marks have been used in forensic investigations for some time, automated skin mark identification is still focused on facial marks, which range from temporary marks (e.g., acnes, which may disappear within a few days) to permanent marks (e.g., nevi, which are usually stable for years). RPPVSM are different from facial marks since they are not specific to the face and only skin marks which are stable for six months or longer are considered as RPPVSM. RPPVSM are also different from birthmarks since birthmarks are congenital (i.e., appear at birth or shortly after birth) but RPPVSM can be congenital or acquired. In fact, most RPPVSM are acquired. Nevi develop during childhood and adolescence, lentigines occur on body sites with a long history

Manuscript received June 2, 2014; revised September 20, 2014. This work was supported in part by the Ministry of Education, Singapore.

A. Nurhudatiana and A.W.K. Kong are with the School of Computer Engineering, Nanyang Technological University, Block N4, Nanyang Avenue, Singapore 639798 (phone: (65) 6513 8041; e-mail: arf0002@e.ntu.edu.sg; adamskong@ntu.edu.sg). A. Nurhudatiana is also with the Program of Information Systems, Binus University International, Jalan Hang Lekir 1 No. 6, Jakarta Indonesia 12270.

of sun exposure, and cherry hemangiomas and seborrheic keratoses usually develop at the age of thirties and forties [10], [11].

Even though skin marks in evidence images can be detected manually by investigators or expert witnesses, it is nearly impossible to process criminal databases manually due to their large size and complexity. To address this problem, an automated RPPVSM identification system which is comprised of skin segmentation, RPPVSM detection, and RPPVSM matching algorithms is proposed in this paper. In addition, a fusion scheme integrating RPPVSM with vein patterns for multimodal identification is also proposed. The fusion is especially useful for Asian population since many Asian subjects tend to have only a few RPPVSM in their bodies [6].

Several skin mark detection and matching methods have been proposed for face recognition systems. In these systems, skin marks are used as additional discriminative features (e.g., to discriminate monozygotic twins) or alternative identification features when face recognition fails (e.g., due to occlusions) [12]-[16]. The first work was by Lin and Tang [12], who decomposed high resolution face images into four different layers — global face appearance, individual face organs (e.g., eyes, nose, and mouth), skin of forehead and cheek, and irregular details (e.g., skin marks). The irregular details were detected and matched using a SIFT-activated pictorial structure, which combines the Scale Invariant Feature Transform (SIFT) for detecting and describing the local interest regions on the face [17], and a pictorial structure for modeling the spatial configuration of the detected irregularities [18]. Their method focused on nevi, which were considered common and prominent enough to be repeatedly detected in different images of the same person.

Another work was by Pierrard and Vetter [13], who detected facial nevi in two steps. First, multi-scale Laplacian of Gaussian (LoG) filters were used as templates to perform normalized cross-correlation matching on illumination-compensated face images. Then, false positives due to non-skin features (e.g., hair strands) were removed by skin segmentation and other false positives due to facial organs (e.g., corners of the eyes, mouth, and nostrils) were removed by a saliency threshold based on size, contrast, and texture features. To perform matching in a pose-independent manner, the locations of nevi in different images were then encoded into a face-centric coordinate system using a 3D Morphable Model [19].

Zhang et al. [14] detected facial marks in a semi-automated fashion by manually labeling seed pixels of facial marks and using region growing operations to grow the seeds of the selected facial marks from one pixel into a group of pixels with similar intensity. The detected facial marks were then matched by taking the normalized location coordinates, area, and the average intensity as features.

Park and Jain [15] introduced facial marks together with gender and ethnicity as soft biometric traits to improve the performance of face matching and retrieval. In their method, ten categories of facial marks, which include freckle, mole, scar, pockmark, acne, whitening, dark skin, abrasion, wrinkle, and other, were automatically detected using a LoG filter with

a kernel size of 3×3 and $\sigma = \sqrt{2}$ and categorized based on their morphology and contrast features. A generic face mask was created using the Active Appearance Model (AAM) [20] to suppress false positives due to primary facial features (e.g., eyes, nose, and mouth). The LoG-filtered image was then subtracted with a user-specific mask, which was created using a Sobel edge filter, to remove user-specific features such as beard and wrinkles around the mouth and eyes [21]. Facial marks were then segmented by a binary thresholding operation. Together with the gender and ethnicity of the subject, the location, morphology, contrast, and frequency of the detected facial marks were then encoded into a histogram and matched using histogram intersection. The soft-biometric matcher was evaluated through a fusion with a state-of-the-art face matcher using a weighted score-sum rule with min-max normalization [22].

Srinivas et al. [16] used facial marks as a standalone biometric for identifying monozygotic twins. Eleven types of skin marks, including some of the facial marks employed in [15] were detected from high resolution images by using an approach similar to [15]. First, a mask describing primary facial features was created using the Active Shape Model [23]. Facial marks were then detected on masked face image using fast radial symmetry transform (FRST) operators [24] in different scales using the Gaussian pyramid technique [25]. Only facial marks which were present at two or more pyramid levels were retained for matching. The facial marks were then segmented through a thresholding operation and their locations were transformed to the Barycentric coordinate system [26], which is a normalized coordinate system based on a reference triangle formed by eye and nose positions in the face [27]. Matching was performed by using the weighted bipartite graph matching method with locations and categories of the facial marks as features.

In addition to face recognition, automated skin mark detection has also been proposed for melanoma diagnosis, where new appearance or disappearance of nevi and changes in pre-existing nevi [28] are observed through regular screenings of patients. Cho et al. [29] detected nevi by applying multi-scale Difference of Gaussian (DoG) filters separately to the R, G, and B channels of input images and considering the set union of the output maxima over different scales and channels as nevus candidates. Subsequently, each detected candidate was classified as nevus or non-nevus by a trained support vector machine. Lee et al. [30] detected nevi on human backs as a part of a study to evaluate the effectiveness of sunscreen for melanoma prevention. Nevus candidates were detected by a mean shift filtering operation [31] followed by a region growing operation. Finally, each nevus candidate was classified as true nevus or other based on a predefined set of measurements, including area, diameter, and contrast. Several skin mark registration methods have also been proposed to monitor nevi automatically [32]-[37]. However, they are not suitable for criminal identification because they are targeted on images of patients which are usually captured in standardized image capture environments.

The proposed RPPVSM identification system differs from the existing facial mark identification methods [12]-[16] in the

following aspects. First, the system is neither specifically targeted on nevi as in [12], [13] nor many categories of skin marks as in [15], [16]. It is targeted on pigmented and vascular skin marks and to realize this purpose, several classifiers were trained using a dermatologist-labeled dataset to classify skin marks as RPPVSM and non-RPPVSM. Second, the proposed RPPVSM identification system does not employ specific face-centric coordinate systems as in [12]-[16] and the matching algorithm is applicable to various body parts (e.g., back, chest, forearm, and thigh).

In the preliminary version of this work [38], skin segmentation was carried out manually and the RPPVSM identification method was evaluated on a small database containing 196 images of backs from 98 subjects. In this work, a significantly larger database, which consists of 3,560 images of backs, chests, forearms, and thighs collected from 400 Caucasian and Asian subjects, has been constructed. A clustering-based skin segmentation algorithm has been developed to automatically preprocess the significantly larger database used in this work. The preliminary version of the RPPVSM detection algorithm has also been improved by modifying the previous static thresholding operation to a dynamic approach. In addition, a fusion scheme between RPPVSM and vein patterns for a multimodal identification is also proposed in this paper. Recently, vein visualization methods to uncover blood vessel patterns hidden in color skin

images were proposed for forensic analysis [52]-[54]. The methods are applicable to the chest, arm, and thigh of the human body where superficial veins are present. Previous study reported that Asian subjects tend to have fewer RPPVSM than Caucasian subjects [6]. Although there are usually sufficient numbers of RPPVSM on the backs for identification, often, there are not many RPPVSM on the forearms and thighs of Asian subjects. Therefore, two experimental settings were used. The first experimental setting treated RPPVSM on the backs as a standalone biometric for unimodal identification, while the second experimental setting fused RPPVSM on the chests, arms, and thighs with vein patterns for multimodal identification.

The proposed RPPVSM identification system and the fusion scheme are illustrated in Fig. 1(a) and (b) respectively. In Fig. 1(a), given an input RGB image of a back, skin segmentation followed by back region localization is performed so that further processing is focused on the back only. RPPVSM are then detected from the segmented image. The detected RPPVSM pattern in the input image is then matched with another RPPVSM pattern retrieved from a prisoner database or extracted from an arrested suspect. A matching score is then calculated to determine the similarity between the two RPPVSM patterns. In Fig. 1(b), given an input RGB image of a forearm, a thigh, or a chest, vein visualization methods are used to visualize the hidden blood vessel pattern in the RGB

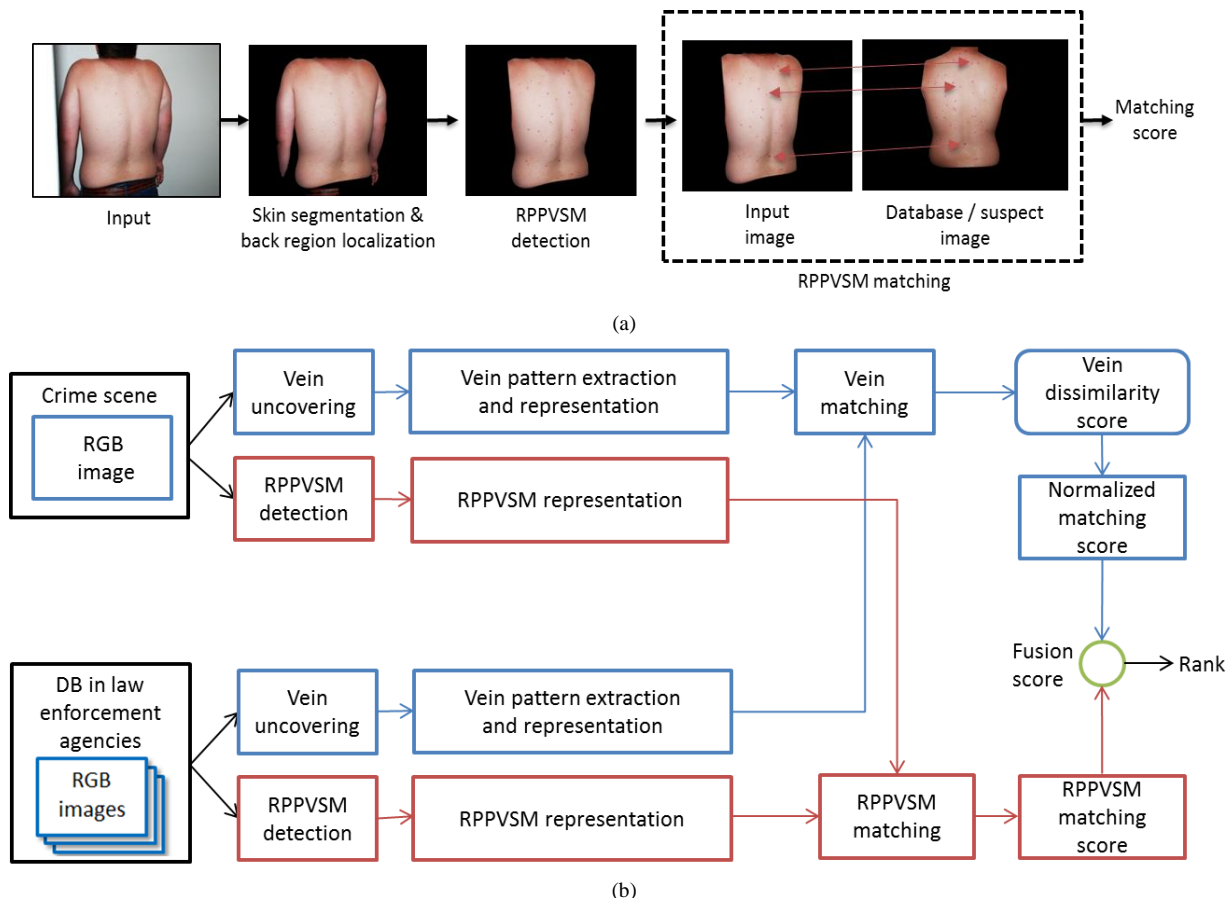


Figure 1. (a) The proposed RPPVSM identification system which consists of skin segmentation, RPPVSM detection, and RPPVSM matching algorithms and (b) the proposed fusion scheme based on RPPVSM and vein patterns.

image. The visualized vein pattern is then extracted and matched with another vein pattern in a database to obtain a vein dissimilarity score [54]. The RPPVSM in the image are also detected and matched using the proposed RPPVSM identification system. Both biometric modalities are then fused at the matching score level by first normalizing the vein dissimilarity score and then combining it with the RPPVSM matching score to produce a fusion score. Lastly, the system returns top- N ranked matches based on the fusion score.

The remainder of this paper is organized as follows. Sections II to IV discuss respectively the skin segmentation, RPPVSM detection, and RPPVSM matching algorithms which form the RPPVSM identification system. Section V describes the fusion scheme with vein patterns. Section VI provides experimental results and discussions. Finally, section VII offers conclusion.

II. SKIN SEGMENTATION

Many of the existing skin segmentation methods can be categorized into the skin color detection approach or the image

segmentation approach [39]-[44]. The skin color detection approach uses statistical methods such as histogram and Gaussian mixture model to define the ranges of skin color values in various color spaces. Using the developed model, skin regions in images are localized by thresholding, look-up table, naïve-bayes classifier, or more complex pattern recognition techniques [39]-[41]. On the other hand, the image segmentation approach applies general image segmentation techniques such as clustering, thresholding, edge detection, and region-growing to divide image into different regions based on the discontinuity or homogeneity of the pixel values in the image [42]-[44]. In this research, skin segmentation algorithm is used as a preprocessing step to suspect databases, such as the prisoner databases and the sex offender registries, which are usually collected in controlled environments. These database images demand much more automatic processing than evidence images collected from crime scenes, which can be processed manually or semi-automatically by forensic officers.

RGB images were collected for algorithm development and

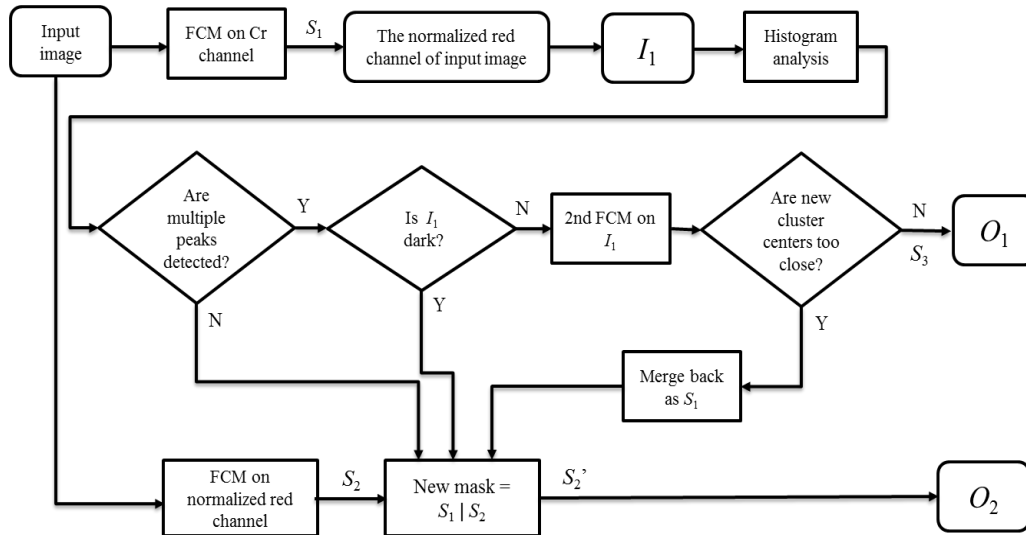


Figure 2. A schematic diagram of the proposed skin segmentation algorithm.

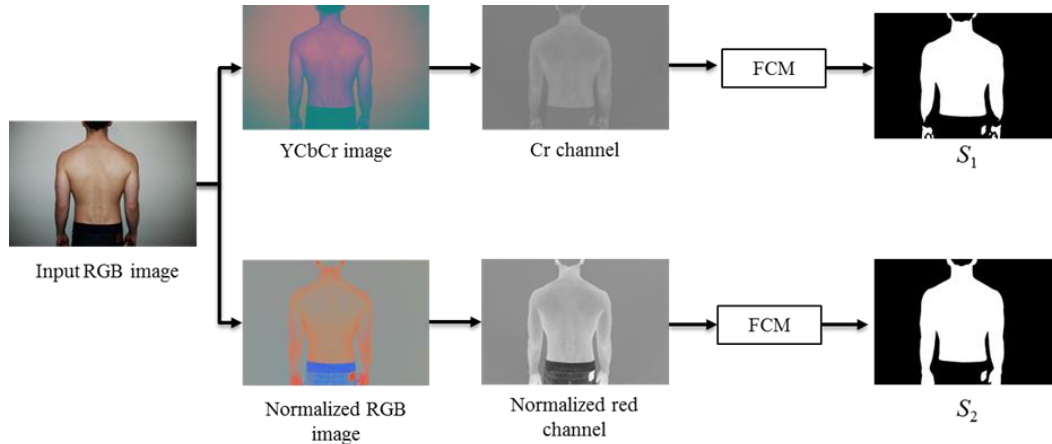


Figure 3. An illustration of the Fuzzy C-Means (FCM) clustering operation on the Cr and normalized red channels and the generated skin masks S_1 and S_2 respectively.

system evaluation purposes. To simulate a suspect database, images were collected in a standard pose and viewpoint condition, while to simulate evidence, images were collected in varying pose and viewpoint conditions. Two common characteristics were observed from the images collected in the standardized setting. First, pixels of skin representing different parts of the human body (e.g., back, chest, arm, and thigh) form homogeneous groups of pixels in the images, and second, skin is usually the largest homogeneous region in the images. Based on these two properties, the Fuzzy C-Means (FCM) algorithm [45], which is a popular clustering method, was adopted for skin segmentation.

The skin segmentation algorithm is illustrated in Fig. 2. Given an input RGB image, the image is transformed into the YCbCr and normalized RGB color spaces because the high Cr coordinates of the CbCr two-dimensional plane in the YCbCr color space localizes skin colors and the normalized RGB color space removes the effect of illumination variations. The normalized RGB color space is defined as

$$\begin{aligned} \text{normR} &= R/\sqrt{R^2+G^2+B^2}, \\ \text{normG} &= G/\sqrt{R^2+G^2+B^2}, \\ \text{normB} &= B/\sqrt{R^2+G^2+B^2}, \end{aligned} \quad (1)$$

where R, G, and B are the intensity values of the red, green, and blue channels respectively.

The Cr and normalized red channels are then extracted from the corresponding color spaces and smoothed using a mean filter. FCM clustering operation with two clusters is then applied to the two channels. Since skin tends to have high intensity values in the Cr and the normalized red channels, the cluster centers are initialized with 10 and 90 percentiles of the intensity values in each channel, where the first cluster represents the background and the second cluster represents the skin. The results given by the FCM clustering operations on the Cr and the normalized red channels are denoted as skin masks S_1 and S_2 respectively (see Fig. 3).

The skin mask S_1 , which is more accurate at localizing skin color than S_2 , is then applied to the normalized red channel of the input image to obtain skin-segmented image I_1 , where the values of the pixels belonging to the first cluster (background)

are set to zero and the values of the pixels belonging to the second cluster (skin) are retained. To check if further FCM operation is required, a histogram analysis is performed to the non-zero intensity values in I_1 . Histogram peaks are detected from bins which satisfy the following criteria: 1) the number of pixels in the bin is greater than or equal to a threshold α , 2) the intensity value difference between the bin and any other bin which is also considered a peak is greater than or equal to a threshold β , and 3) the bin distance between the bin and any other peak is greater than or equal to a threshold γ . In the experiment, the number of bins was set to 30, the value of α was set to 5% of the total number of non-zero pixels in the image, and the values of β and γ were set to 0.065 and 3 bins respectively. If the number of the detected peaks is greater than one, there is possibly another object with a relatively similar color as skin in the image. Fig. 4 shows two sample images with plain and more complex backgrounds. The histogram of the first image has only one peak and the histogram of the second image has two peaks.

If multiple peaks are detected, dark region checking is first performed by searching for any peak in I_1 with an intensity value less than a threshold δ (set to 0.85 in the experiment). This is because skin in the Cr channel tends to be partially segmented in non-uniform and low (dark) illumination conditions and thus should not be segmented further. If the skin-segmented image I_1 does not contain any dark region, I_1 is further segmented by repeating the FCM clustering operation with two clusters. If the intensity value difference between the two new cluster centers is greater than a threshold ε (set to 0.10 in the experiment), the smaller cluster is removed and the larger cluster is retained based on the previously mentioned assumption that skin is usually the largest homogeneous region in the image, resulting in a new skin mask S_3 . S_3 is then applied to the input image to produce the final skin-segmented image O_1 . Otherwise, the two clusters are merged back as S_1 since their intensity values are too close. If S_3 is not generated as the final skin mask, S_1 and S_2 are combined using the OR operator to produce the final skin

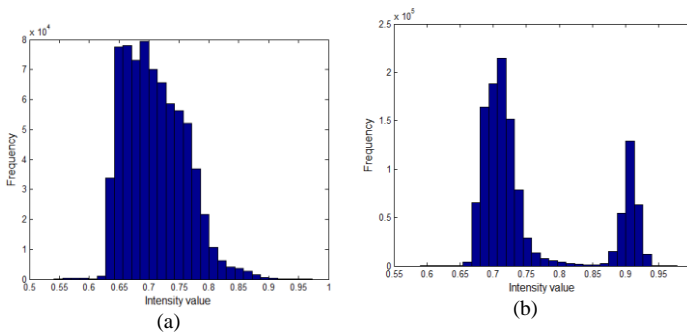


Figure 4. An illustration of the histograms obtained from two input images with (a) plain and (b) more complex backgrounds; (a) shows one histogram peak and (b) shows two histogram peaks.

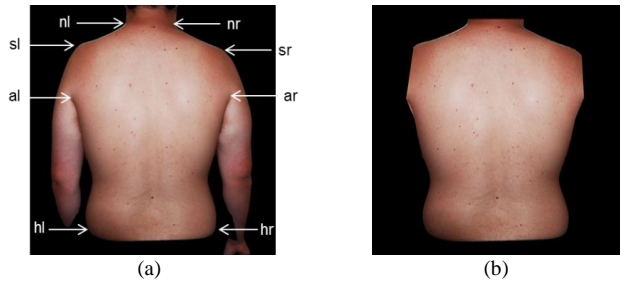


Figure 5. A standard back shape for registration; (a) the human torso template defined by eight anatomical landmarks: neck-left (nl), neck-right (nr), armpit-left (al), armpit-right (ar), shoulder-left (sl), shoulder-right (sr), hip-left (hl), and hip-right (hr); (b) the segmented back.

mask S_2' and applied to the input image to produce the final skin-segmented image O_2 . To obtain a smooth segmentation result, morphological filtering operations are first applied to the final mask before it is applied to the input image.

Since RPPVSM matching is to be performed on specific body parts (e.g., back is matched to another back and forearm is matched to another forearm), a standard shape of the back is extracted based on the human torso template proposed in [37]. The template is defined by eight anatomical landmarks – neck-left (nl), neck-right (nr), armpit-left (al), armpit-right (ar), shoulder-left (sl), shoulder-right (sr), hip-left (hl), and hip-right (hr) (see Fig. 5(a)). The eight anatomical landmarks are automatically detected using a curvature scale space corner detector with an adaptive threshold technique [49]. If the detected landmarks are not correct, for example due to pose and viewpoint variations, manual corrections are made. The landmark pairs (al)-(sl) and (ar)-(sr) are then used to segment out the left and right upper arms respectively and the landmark pair (nl)-(nr) is used to segment out the head from the back template (see Fig. 5(b)).

III. RPPVSM DETECTION

RPPVSM are automatically detected from the skin-segmented image in three steps – preprocessing, RPPVSM candidate detection, and classification (see Fig. 6). Given a skin-segmented RGB image, its blue channel is extracted and normalized by adjusting its intensity values to range between 0 and 1. Blue channel is used because skin marks, located at the surface of the skin, are more sensitive to the wavelengths of the blue channel compared to the wavelengths of the green and red channels, which penetrate into the deeper layers of the skin. A homomorphic filter [46] is then applied to the blue channel image to normalize its brightness and increase its contrast.

RPPVSM candidates with different sizes are detected by Laplacian of Gaussian (LoG) filters with five different scales ($\sigma = \sqrt{2}, 2, 4, 6, 8$) and a kernel size of 20x20. An optimal response image defined as

$$IM_{opt}(x, y) = \max_s IM_{LoG_s}(x, y), \quad (2)$$

where IM_{LoG_s} is the response image from the LoG filtering operation with scale s , is then inverted so that the RPPVSM candidates appear darker than the surrounding skin pixels. To enhance the RPPVSM candidates, a third rank-order filter with a kernel size of 5x5 is applied to the optimal response image. The third rank instead of the first rank is used to avoid amplifying the noise together with the RPPVSM candidates. RPPVSM candidates in the enhanced image are subsequently segmented from the neighboring skin by a thresholding operation as follows:

$$L(x, y) = \begin{cases} 1 & \text{if } t_1 \leq I(x, y) \leq t_2 \\ 0 & \text{otherwise} \end{cases} \quad (3)$$

where $L(x, y)$ is a binary label of a pixel at (x, y) coordinate, I is the grayscale image obtained after the rank-order filtering

operation, and t_1 and t_2 are minimum and maximum thresholds, which are initialized with 0.01 and 0.35 respectively. The maximum threshold t_2 is used to remove regions with weak LoG filtering responses and the minimum threshold t_1 is used to exclude body boundary.

To improve the preliminary method [38], which used a static thresholding approach and thus was not robust to illumination and contrast variations, a dynamic thresholding approach is developed. The dynamic thresholding operation starts with the initialized values of t_1 and t_2 and then repeats iteratively with $t_2 = t_2 + 0.01$ at each iteration. The iteration stops when the number of newly detected RPPVSM candidates at a new iteration is greater than a threshold value t_3 or the maximum number of iterations t_4 is reached. In the experiments, t_4 was set to 5 and t_3 was set to 2 for the thighs and forearms, 5 for the chests, and 8 for the backs. Different values of t_3 were used since the area of skin and the average number of RPPVSM in each body part are different.

Hair strands, which are often present in the upper and lower parts of the back, are sometimes detected as RPPVSM candidates. To remove them, a simple density analysis is performed by dividing the image into grids with equal sizes and counting the number of RPPVSM candidates in each grid. Since hair strands tend to be located near each other, they can be detected from grids where the numbers of RPPVSM candidates are unusually large. In the experiment, each back image was divided into 40 grids. Grids with numbers of RPPVSM candidates exceeding a threshold τ ($\tau = t_3$) were considered containing hair strands. The RPPVSM candidates in these grids were thus excluded from further processing.

In the last step, RPPVSM candidates are classified as true RPPVSM or non-RPPVSM (e.g., acne, pore, and hair) based on their contrast, shape, size, texture, and color features. For measuring the contrast, two bounding boxes BB_1 and BB_2 are constructed (see Fig. 7). The first bounding box BB_1 encloses the detected RPPVSM candidate, while the second bounding box BB_2 encloses the neighboring area of BB_1 with a distance of p pixels ($p = 2$ in the experiment). The contrast value is described by two parameters c_1 and c_2 defined as

$$c_1 = \frac{1}{N} \sum_{i \in BB_1} I_i \quad \text{and} \quad c_2 = \frac{1}{M} \sum_{j \in BB_2 \setminus BB_1} I_j, \quad (4)$$

where N is the number of RPPVSM candidate pixels in BB_1 , M is the number of pixels in BB_2 not including BB_1 (i.e., $BB_2 \setminus BB_1$), and I_i and I_j are the intensity values of the i^{th} and j^{th} pixels, respectively. c_1 is the mean intensity value of the RPPVSM candidate enclosed in BB_1 and c_2 is the mean

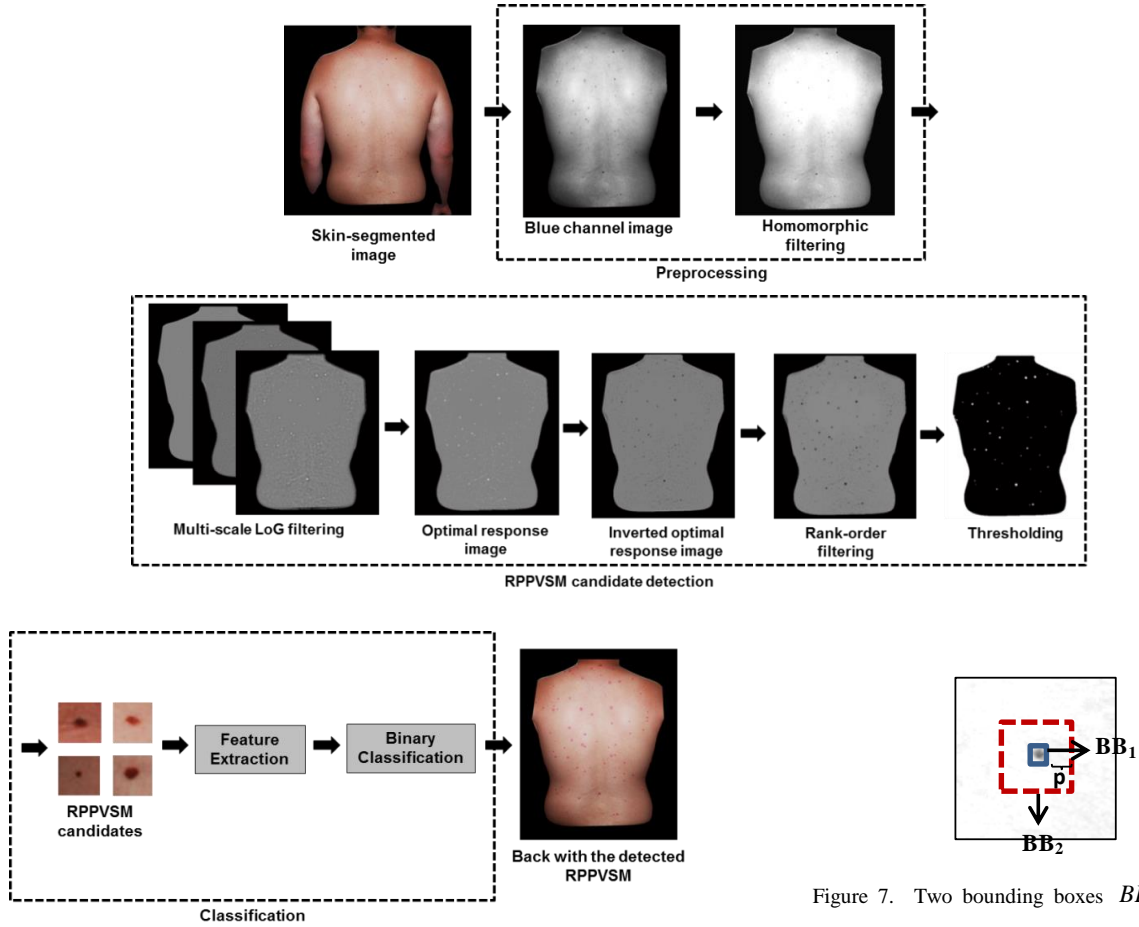


Figure 6. An illustration of the RPPVSM detection algorithm.

intensity value of the neighboring skin. Both c_1 and c_2 are calculated from the contrast-enhanced image after the homomorphic filtering operation.

Since RPPVSM are usually circular, their shape can be described using three elliptical properties — eccentricity, major axis length, and minor axis length. Given an elliptical object, the eccentricity is defined as

$$e = \sqrt{1 - \frac{b^2}{a^2}}, \quad (5)$$

where a is the major axis length and b is the minor axis length. An eccentricity value of zero indicates a circle while an eccentricity value of one indicates a line segment. The size feature is defined as the number of connected pixels in a RPPVSM candidate. Texture feature is obtained by applying the rotationally invariant uniform Local Binary Pattern (LBP) [47] on the bounding box BB_2 . The rotational invariant uniform LBP operation leads to 10 different values (0, 1, 2, ..., 9), which are represented as a 10-bin normalized histogram. The color feature is described using the minimum, maximum, and average normalized intensity values of the R, G, and B channels. Finally, for each RPPVSM candidate sample, a feature vector of length 25 is extracted for classification (i.e., 2 from contrast, 3 from shape, 1 from size, 10 from texture, and 9 from color).

Figure 7. Two bounding boxes BB_1 and BB_2 for measuring the contrast feature.

Three common learning-based classifiers which include decision tree, three-layered feed-forward neural network, and support vector machine (SVM), were used to perform the classification. The Gini's diversity index [48] was utilized as the split criterion for the decision tree. The neural network was implemented with 10 neurons in the hidden layer and tan-sigmoid transfer functions in the hidden and output layers. The neural network was trained using the scaled conjugate gradient backpropagation algorithm. The SVM was implemented with the linear kernel function.

To train the classifiers, the image database was divided into training and testing datasets. Positive samples (i.e., RPPVSM) were obtained by asking dermatologists to manually label RPPVSM on 20 back images of Caucasian and Asian subjects. Negative samples (i.e., non-RPPVSM) were obtained by applying the preliminary RPPVSM candidate detection technique to the same 20 back images [38]. The detected RPPVSM candidates not labeled as RPPVSM by the dermatologists were then employed as negative samples. Finally, 234 samples of RPPVSM and 628 samples of non-RPPVSM were used to form the training dataset. All of the three classifiers were trained on the same dataset.

IV. RPPVSM MATCHING

Two processes are involved in RPPVSM matching. First is

RPPVSM pattern registration, where a standard shape of the back, which was extracted from the back image after the skin segmentation, is employed to obtain proper alignment between two RPPVSM patterns. The boundary of the segmented back is detected using the Roberts edge detector [50] and down-sampled to form a point set. RPPVSM are then combined with the boundary points for registration, which is performed using the non-rigid Coherent Point Drift (CPD) point matching method [51] (see Fig. 8). After the input and template RPPVSM patterns are aligned, matching score calculation is performed. The k -Nearest Neighbor algorithm with $k = 1$ is used to search for correspondences. A correspondence between two RPPVSM, where one is from the input and the other one is from the template, is established if $d \leq r_0$, where d is the distance between the two RPPVSM and r_0 is a tolerance distance parameter. Finally, the matching score defined as $2c / (m + n)$, where c is the number of correspondences, m is the number of RPPVSM in the template pattern, and n is the number of RPPVSM in the input pattern, is calculated. In the experiment, r_0 was determined from

$$\Pr(3 \times \text{major axis length of RPPVSM} \leq r_0) \geq t, \quad (6)$$

where t is a statistical threshold. The tolerance distance parameter r_0 was set to 30 pixels based on $t = 95\%$.

Since three different classifiers are used for RPPVSM detection, three matching scores, each from a different classifier, are obtained. A fusion is performed to obtain better matching performance. The fusion uses a weighted sum rule given by

$$s_{\text{fusion}} = \frac{w_{SVM} \times s_{SVM} + w_{NN} \times s_{NN} + w_{DT} \times s_{DT}}{w_{SVM} + w_{NN} + w_{DT}}, \quad (7)$$

where w_{SVM} , w_{NN} , and w_{DT} are weights assigned to different classifiers and s_{SVM} , s_{NN} , and s_{DT} are the matching scores given by the classifiers.

V. FUSION WITH VEIN PATTERNS

As mentioned before, one problem with using RPPVSM for identification is that its effectiveness depends on the number of RPPVSM available. A RPPVSM pattern formed by only a few RPPVSM is not sufficient to uniquely identify a person. This problem is more obvious in Asian subjects since they do not usually have many RPPVSM on their skin [6]. Moreover, the numbers of RPPVSM on the arms and thighs tend to be lower

than the numbers of RPPVSM on the backs and chests. Recently, there have been some research efforts to visualize vein patterns of non-facial body parts hidden in color images for forensic analysis [52]-[54]. Vein pattern is a useful biometric trait due to its universality, permanence, and uniqueness. To alleviate the problem of identification with a limited number of RPPVSM, a fusion scheme which combines RPPVSM with vein patterns for multimodal identification on chests, arms, and thighs is presented in this section. The fusion scheme adopts the proposed RPPVSM identification system presented in the previous sections and a preliminary version of the vein uncovering algorithm presented in [54]. We used the preliminary version because the vein uncovering algorithm in [54] was developed simultaneously with this work. To provide a complete description of the multimodal system, an overview of the vein identification system is given in the following subsections.

A. Vein Identification in Color Images

While vein patterns underneath the skin can be seen in near infrared (NIR) images, they are usually invisible in RGB images. Therefore, the first step of vein identification is to visualize the hidden vein patterns in the input RGB image using a vein uncovering method [52]. The uncovered vein patterns is then extracted using a Gabor filtering-based vein pattern extraction method and represented in a point set for matching [53]. The vein pattern point set is then matched with other vein patterns in a database using a 3-step vein pattern registration method, which includes a registration of the arm boundary, a registration of vein patterns, and a registration of vein patterns to determine correspondence points [53]. Finally, a vein dissimilarity score based on distance and vein segment orientation differences is calculated [61]. Fig. 9 illustrates the vein identification system.

To visualize vein patterns, the preliminary version of the vein uncovering method recently proposed by Sharifzadeh et al. [54] is employed. The method is a further development of the image mapping method proposed by Tang et al. [62]. The vein pattern visualization process used in this paper is illustrated in Fig. 10. First, an input image goes to a preprocessing stage, where the illumination in the image is adjusted in the LAB color space and the contrast is adjusted in the RGB color space using the contrast-limited adaptive histogram equalization method. Then, a three-layered feed-forward neural network which was previously trained on pairs of synchronized preprocessed RGB and NIR images of the skin was used to map the RGB values in the preprocessed

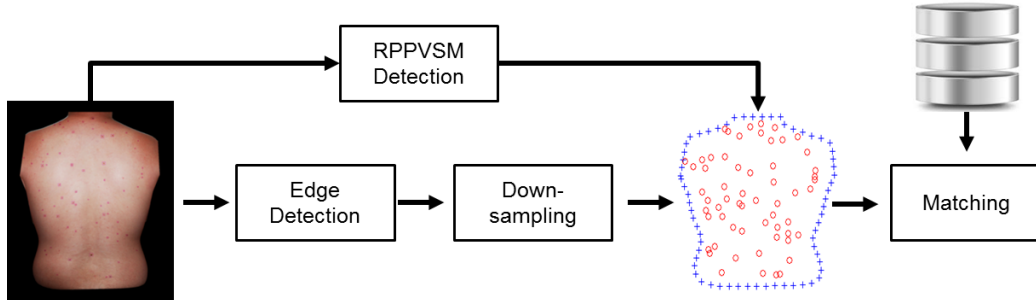


Figure 8. Registration point set generation for RPPVSM matching. The blue crosses and the red circles represent the boundary points and the detected RPPVSM respectively.

input images to NIR intensity values which contain vein information. The synchronized color and NIR images were taken using a 2-CCD multispectral camera. The camera simultaneously captures images in visible and NIR light spectrums through a single lens with two channels – a Bayer mosaic color imager and a monochrome NIR imager. Before the images were used to train the neural network, the color images went through the same preprocessing step for the input images mentioned before and the synchronized NIR images were enhanced using a Gabor filtering operation. Since it was noted that the trained neural network was affected by illumination variation, especially at the green channel, a weight adjustment parameter based on the average size of vein segments in the skeletonized image was added to the green channel at the input layer of the neural network [62]. The neural network was trained using the back propagation method with 5 hidden neurons.

B. RPPVSM Matching in the Fusion

To match RPPVSM on the chests, the same human torso template and non-rigid CPD method for matching RPPVSM on the backs are used. However, since predefined regions of

interest (ROI) are used for matching vein patterns in forearms and thighs, a different RPPVSM matching scheme is designed for these two body parts.

For the vein identification system, the ROI for the forearm is defined as from elbow to wrist and the ROI for the thigh is defined as from knee to around 30 cm below the hip. The images are rotated and resized to 1024x357 pixels for the forearm and 1,118x636 pixels for the thigh such that they can be compared in similar scales and positions. To match the RPPVSM on these two body parts, the locations of RPPVSM are encoded into a normalized coordinate system with a range of $[-1, 1]$ in both vertical and horizontal directions (see Fig. 11). The k -Nearest Neighbor algorithm with $k = 1$ is used to find RPPVSM correspondences between the input and template images in the normalized coordinate system. Since the same RPPVSM in the input and template images do not always lie on the same normalized coordinates due to posture variations, a match is established if $d \leq r_0$, where d is the Euclidean distance between the two RPPVSM and r_0 is a tolerance distance parameter in the normalized coordinate system. r_0 was set to 0.20 in the experiment.

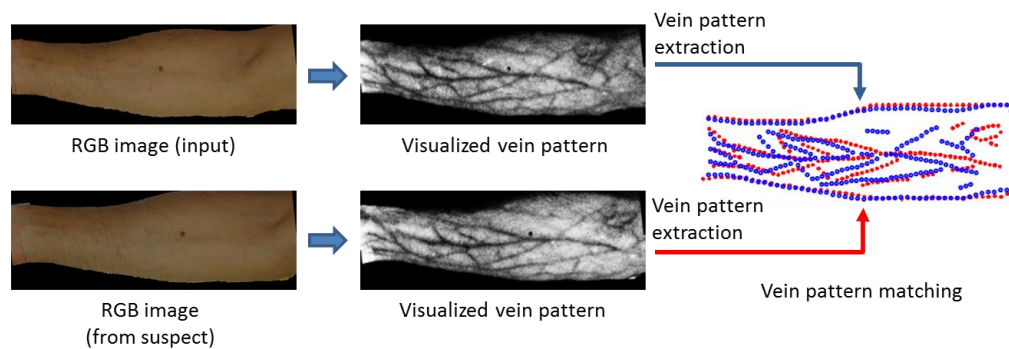


Figure 9. Illustration of the vein identification system

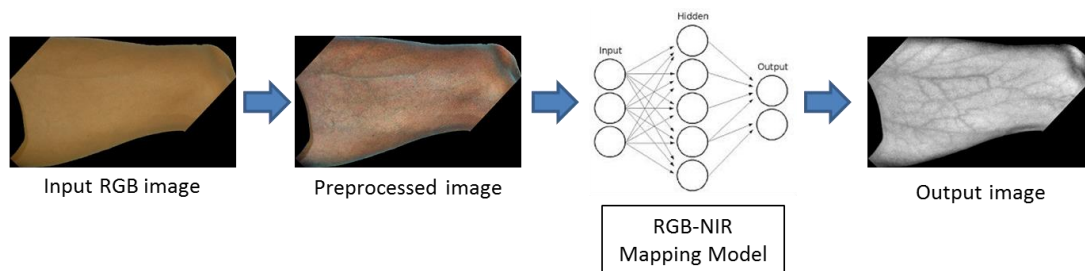


Figure 10. Illustration of vein visualization process using the vein uncovering method in [54].

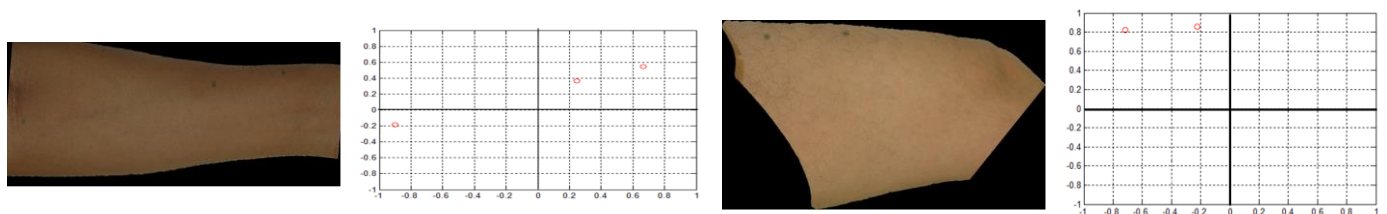


Figure 11. Presegmented (a) forearm and (b) thigh used in vein identification and the normalized coordinate system for RPPVSM matching. The red circles represent the locations of RPPVSM.

The matching score calculation given in section IV is not suitable for patterns with limited RPPVSM. For example, when matching a forearm image with two detected RPPVSM, if one of them is not detected in the correspondence image (e.g., due to poor contrast), the matching score will decrease by half. Therefore, in the fusion, the matching score calculation is changed to $0.1 \times c$, where c is the number of RPPVSM correspondences. Among the three classifiers, only one classifier which gives the best identification on the backs is used.

C. Fusion Score Calculation

To fuse the vein and RPPVSM matching scores, the vein dissimilarity score is first normalized to range between 0 and 1, where 0 indicates non-match and 1 indicates a perfect match. Since it was observed that the vein dissimilarity scores typically range between 0 and 200, the normalization is given by

$$s_{vn} = 1 - \left(\frac{s_v}{200} \right), \quad (8)$$

where s_{vn} is the normalized vein matching score and s_v is the vein dissimilarity score. The RPPVSM matching score is then fused with the normalized vein matching score using the following rule. Given matching scores of vein and RPPVSM patterns, if the vein patterns match very well (i.e., the normalized vein matching score is 0.85 or higher), the fusion score is calculated as $s_f = s_{vn} + 0.2s_r$, where s_r is the RPPVSM matching score, to emphasize the contribution by the vein matching score; otherwise, the fusion score is calculated as $s_f = s_{vn} + s_r$. Finally, the identification results are retrieved in a ranked order based on the fusion scores.

VI. EXPERIMENTAL RESULTS AND DISCUSSIONS

To evaluate the RPPVSM identification system and the fusion scheme, two sets of images were collected in two different locations. The first set of images was collected in Los Angeles using a Nikon D80 camera (maximum pixel resolution 3872x2592). It contains 500 images of backs from 100 male subjects, mostly Caucasian, with an average image resolution of 100 dpi. The second set of images was collected in Singapore using a Nikon D70s camera (maximum pixel resolution 3008x2000) and a Canon EOS 500D camera (maximum pixel resolution 4752x3168). It contains over 3000

images of backs, chests, forearms, and thighs from 328 subjects, mostly male Asian including Chinese, Malay, and Indian, with image resolutions ranging from 60 to 150 dpi. Images of backs, chests, forearms, and thighs were taken from the male subjects and only images of forearms and thighs were taken from the female subjects. The images in the second dataset were captured in two different sessions with an interval ranging from one to two weeks. However, most of the images in the first dataset were captured in a single session due to limited availability of volunteers. All the images were captured indoors and the subjects were not given strict pose instructions during the image collection process. Fig. 12 shows examples of the back, chest, forearm, and thigh images in our database.

Since the presence of large tattoos and dense androgenic hair greatly reduced the visibility of RPPVSM, images with large tattoos and dense androgenic hair were excluded. Note that tattoos and androgenic hairs can both be used for identification [56] and thus they can be used as alternative biometric traits when RPPVSM are covered. 1200 back, 460 chest, 500 right forearm, 480 left forearm, 460 right thigh, and 460 left thigh images from a total of 400 subjects were used for evaluation. Before the images were inputted to the system, the back images were first resized to 2000x1330 pixels and the ROIs of the forearm and thigh images were presegmented as explained in section V. For the chest, forearm, and thigh images, the first session images were used as a gallery set and the second session images were used as a probe set. For the back images, one to three images of each subject were assigned to the gallery set while the remaining images, including those with varying poses and viewpoints, were assigned to the probe set. In the following subsections, the results of skin segmentation, unimodal RPPVSM identification on the backs, and the fusion with vein patterns on the chests, forearms, and thighs will be reported.

A. Skin Segmentation

Since skin segmentation serves as a preprocessing step to RPPVSM identification only, visual observation is used to evaluate the quality of the segmentation results. It is generally observed that the segmentation algorithm is effective for the simulated suspect images which were captured in standardized setting. However, for images with more complex backgrounds and poses, which are used to simulate evidence images, manual correction is allowed if the segmentation results are not satisfactory. This is similar to common scenarios in fingerprint identification where latent print is sometimes manually corrected to improve identification.

Fig. 13 shows some images in the database and the

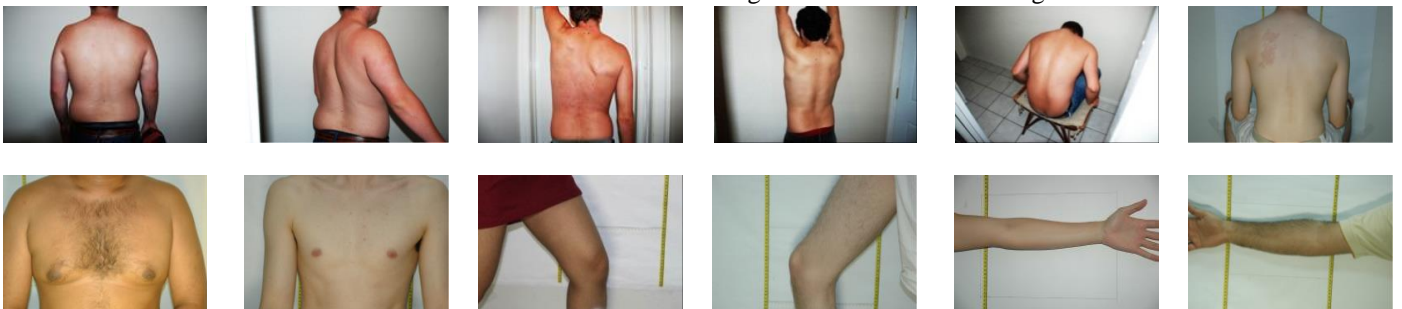


Figure 12. Examples of images in our database.

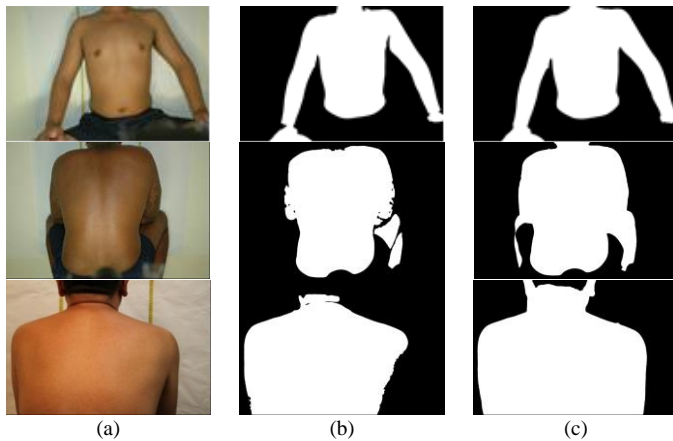


Figure 13. Skin segmentation results; (a) the raw color images, (b) the S_1 masks, (c) the S_2' masks, and (d) the skin-segmented images after applying (c) to (a).

corresponding skin segmentation results. It can be observed that the skin mask S_1 alone can actually be used for skin segmentation in the standard images. However, S_1 is sensitive to dark skin (2nd row) and non-uniform illumination conditions (3rd row). In the 2nd row, S_1 is not smooth around the body boundary, and in the 3rd row, S_1 gives partial skin of the back. These problems are solved after combining S_1 with S_2 as seen in column (c).

Fig. 14 compares S_1 , which is obtained from one clustering operation, and S_3 , which is obtained from two clustering operations, in two input images with more complex backgrounds. In the first skin mask S_1 (left), a non-skin object, which is the wall in the background, is still included in the mask due to similarity in the Cr intensity values with skin color. However, in the final skin mask S_3 (right), the wall is separated from the skin after the second clustering operation and is finally removed based on the assumption that skin is usually the largest homogeneous region in the image.

B. Unimodal RPPVSM Identification on the Backs

The standalone RPPVSM identification system was evaluated on the back images, which included 1,200 images from 283 Caucasian and Asian subjects separated into 420 gallery and 780 probe images. Back was chosen because it covers a large area in the human body and thus tends to have more RPPVSM. Fig. 15 shows the cumulative matching characteristic (CMC) curves of RPPVSM identification using SVM, neural network (NN), and decision tree (DT) classifiers. SVM achieved the best results with rank-1 and rank-10 accuracies of 73.33% and 86.28% respectively, followed by neural network with 71.03% and 84.87%, and decision tree with 54.23% and 76.28%. This is similar to our preliminary finding in [38] that SVM classifier is superior to neural network and decision tree classifiers for RPPVSM identification. To improve the matching performance, Eq. 7

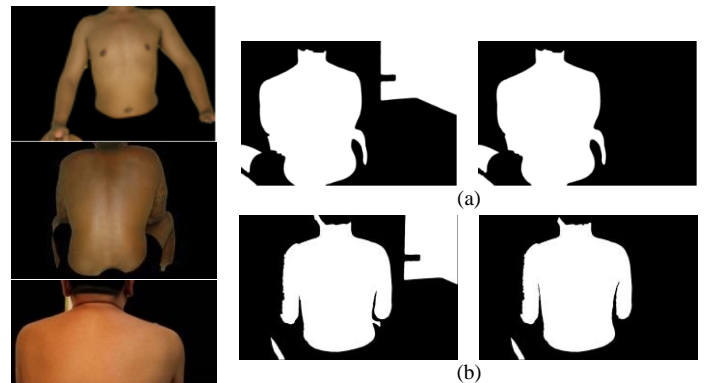


Figure 14. Skin masks S_1 (left) and S_3 (right) from two input images with more complex backgrounds; (a) the first input image, (b) the second input image.

was used to fuse the matching scores produced by the classifiers with the weights set to 3:2:1 for SVM, neural network, and decision tree respectively based on their performance ranking. The score-level fusion improves the rank-1 and rank-10 accuracies to 76.79% and 88.97% respectively (see Fig. 15).

For a practical implementation of the system, instead of performing RPPVSM identification three times, each with a different classifier and fusing their scores afterwards, one may consider using one classifier which gives the best results. However, the fusion scheme is required for achieving better results. In overall, the fusion improves the accuracies of the best classifier, which is the SVM, by around 3%. The system was implemented in Matlab on a 3.20 GHz computer running Windows 7 operating system. The average computation time of the proposed RPPVSM detection algorithm was 6 seconds and the matching algorithm required between 0.05 to 0.20 seconds to match an input RPPVSM pattern with another RPPVSM pattern. Therefore, the computational cost of using three classifiers, each takes the same feature vector as input, is very low, especially if the code is implemented in low-level language, such as C and C++.

As there is no other RPPVSM detection method besides this work and the preliminary work in [38], for comparison purpose, two skin mark detection methods previously proposed for face biometrics are used. Fig. 16 and Table 1 show the performances of the proposed RPPVSM detection algorithm, the preliminary RPPVSM detection method [38], the single-scale LoG filtering method [15], and the FRST-based method [16]. The last two methods were previously proposed for detecting facial marks. In order to have a fair comparison, all the methods were applied to the blue channel of the RGB images. In addition, a LoG filter with a kernel size of 20×20 and $\sigma = 2$, which was the typical size of RPPVSM in the database, was used in the single-scale LoG filtering method [15], and the fast radial symmetry transform (FRST) operators [55] with radii similar to the sizes of the LoG filters used in our algorithm were used in the FRST-based method [16]. The Gaussian pyramid employed in [16] for detecting skin marks with different scales was not implemented because

the radii of the FRST operators were already assigned with the typical sizes of skin marks in the database.

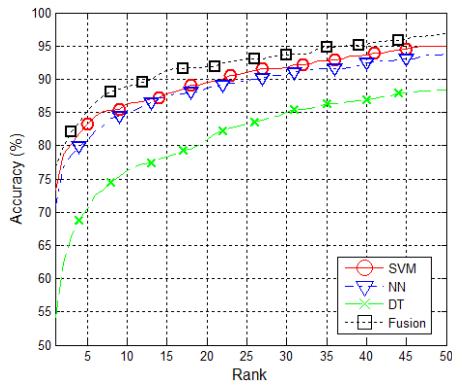


Figure 15. CMC curves of RPPVSM identification using different classifiers and the score-level fusion (Eq. 7).

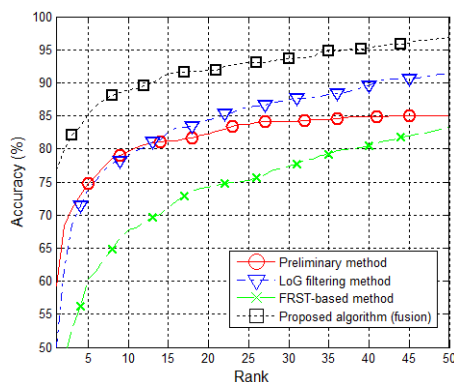


Figure 16. CMC curves of RPPVSM identification using the proposed RPPVSM detection algorithm, preliminary method, single-space LoG filtering method, and FRST-based method.

TABLE I
THE ACCURACY OF THE PROPOSED RPPVSM DETECTION ALGORITHM AND COMPARISON METHODS

| Algorithm | Rank-1 | Rank-5 | Rank-10 | Rank-50 |
|---|---------------|---------------|---------------|---------------|
| Preliminary method [38] | 59.23% | 74.74% | 79.61% | 85.00% |
| Single-space LoG filtering method [15] | 50.13% | 74.10% | 78.97% | 91.28% |
| FRST-based method [16] | 37.31% | 60.26% | 67.82% | 83.20% |
| Proposed algorithm (score-level fusion) | <u>76.79%</u> | <u>85.26%</u> | <u>88.97%</u> | <u>96.92%</u> |

The proposed RPPVSM detection algorithm outperforms all the other methods with significant margins. The RPPVSM classification procedure in the proposed algorithm excludes unstable skin marks, resulting in more stable identification. Moreover, the proposed RPPVSM detection algorithm, which uses a dynamic thresholding approach, handles illumination and contrast variations better and thus increases the rank-1 accuracy of the preliminary method by 17%.

The system has rank-1 and rank-5 identification accuracies of around 77% and 85% respectively, and rank-10 identification accuracy of almost 90%. These results show that the system is useful to search for suspects from a given

database (e.g., prisoner image database), which is a common challenge encountered during the investigations of child pornography and other cases mentioned in section I. In these cases, investigators often rely heavily on digital images as the primary evidence for identification without any information of other biometrics. The rank-10 of the proposed RPPVSM identification system, which includes the real criminal at almost 90% of the time, can be used as a starting point to search for potential suspects or reducing the number of suspects. As this is the first work of human identification using body skin marks, the proposed system can be further improved in the following years just like other biometric technologies which are continuously improved through many years, for example fingerprint [57].

To evaluate the system in a large-scale identification scenario, simulated patterns were added to the gallery set. The probe set still contained 780 images from 283 subjects, but the number of RPPVSM patterns in the gallery set was increased to 1220 which included 420 real patterns from the 283 subjects and 800 simulated patterns representing 800 different subjects. Since most Asians have fewer than 50 RPPVSM on their backs and that their RPPVSM patterns tend to follow homogeneous Poisson distribution [7], each of the simulated patterns was generated from the homogeneous Poisson distribution in the following way. First, a random back sample was drawn from the 420 real backs in the gallery set. The maximum rectangular area inside the boundary of the back sample was then estimated. The rectangular area was divided into non-overlapping 4-row-by-3-column subregions, where for each subregion, a random number j was drawn from a Poisson distribution with a mean λ ranging from 0.5 to 4. The range of λ was selected such that the number of RPPVSM in each pattern ranges from 6 to 48 (number of RPPVSM = $\lambda \times$ rows \times columns), which according to the statistical result in [7], tend to follow homogeneous Poisson distribution. For each of the j events within each subregion, two values were sampled from uniform distributions and used as the x and y coordinates of the simulated RPPVSM inside the subregion. This procedure was repeated until all subregions were processed.

Fig. 17 compares the CMC curves of the system with the larger gallery sets. Even though the gallery set was increased from 420 images to 1220 images, the identification accuracy is still above 70%. This indicates that the system can handle a relatively large gallery set.

To evaluate the performance of the system in varying pose and viewpoint conditions, Fig. 18 shows the matching results of three different Caucasian subjects in different poses and viewpoints. It can be observed from Fig. 18 that non-linear skin distortions caused by pose and viewpoint variations reduce the matching scores. However, in most cases, the correct images in the gallery set can be retrieved at rank-1 because the numbers of RPPVSM on the backs of these subjects are sufficient to uniquely differentiate them from the rest of the images. It was also observed that the performance of RPPVSM identification is largely influenced by the number of RPPVSM available. Some Asian subjects had only a few

RPPVSM on their backs. The identification in these back images was not as good as in other back images with more RPPVSM.

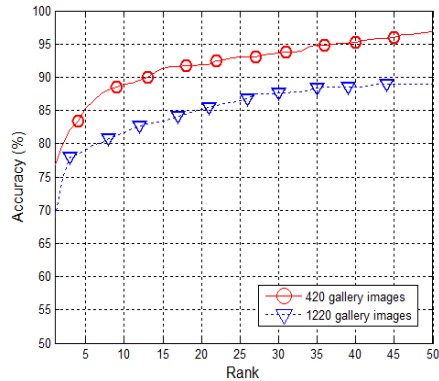


Figure 17. CMC curves from gallery sets containing 420 images and 1220 images.

C. Fusion with Vein Patterns

The fusion between RPPVSM and vein patterns was evaluated on 2,360 images of chests, forearms, and thighs collected from mostly Asian subjects, including Chinese, Indian, and Malay. Chest, arm, and thigh were selected for the fusion because they were obtained from Asian subjects, who tend to have fewer RPPVSM than Caucasian subjects and thus requires the fusion because they cannot be identified by RPPVSM alone. For the experiments, the same inner forearm dataset used in [63] and the same inner thigh dataset used in [61] were used. Back was not included because back does not usually have visible superficial veins.

Fig. 19 shows the CMC curves of vein identification with and without the fusion with RPPVSM. It can be observed that in general, the fusion improves the performance of vein identification on all body parts. The rank-1 accuracies on the chests before and after the fusion are 41.48% and 45.41% respectively. The rank-1 accuracies on the left (right) forearms before and after the fusion are 57.32% (61.60%) and 59.83% (66.00%) respectively. The rank-1 accuracies on the left (right) thighs before and after the fusion are 30.00% (36.84%) and 33.48% (37.28%) respectively. Although the improvement rates at rank-1 accuracies are generally similar for all body parts (2% to 5%), the overall improvement rate is observed to

be higher for the chests. This is because the chest, which covers a large area of the human body, tends to have more RPPVSM than the other two body parts. The number of detected RPPVSM on the chest of each subject ranges from 0 to 17, while the number of detected RPPVSM on the forearm or thigh of each subject ranges from 0 to 6 only.

It is also observed from Fig. 19 (b) that the performance of vein identification on the right forearms is higher compared to the left side. One reason is due to the right-handedness tendency in most people. Because more people use their right arms more frequently, the hardening of muscles in these two body parts causes cutaneous veins near the muscles getting pushed towards the skin, making them more visible [60]. The other reason is due to different sizes of ROI. The ROI of the right forearms are larger than the ROI of the left forearms because some subjects wore watches and accessories on their left wrists and forearms. This makes vein visualization in the right forearms easier and clearer than in the left forearms, resulting in higher vein identification accuracy for the right forearms. Fig. 19 (c) also shows that the performance of vein identification on the right thighs is higher compared to the left side. However, the ROI of the left thighs and the right thighs are similar. It is not expected that the right-handedness tendency has strong effects on thighs, except that the subjects train their left and right thighs differently in some sports, e.g., football, but this information was not collected.

The performance of the above vein identification system, even after the fusion with RPPVSM, is lower than some of the existing finger vein and hand vein biometric systems for commercial applications [58], [59]. However, there is a significant difference between forensic and commercial biometric systems. The main difference between our system, which is targeted for forensic application and the existing finger vein and hand vein recognition systems, which are targeted for the commercial market lies on the image acquisition, feature extraction and user cooperation. First, our system was tested on images which were captured in non-standard-setting environments. This is more challenging than the controlled acquisition conditions employed by commercial systems. Second, in the commercial systems, vein patterns are usually extracted directly from the input infrared images and then matched with template vein patterns in a database. Since

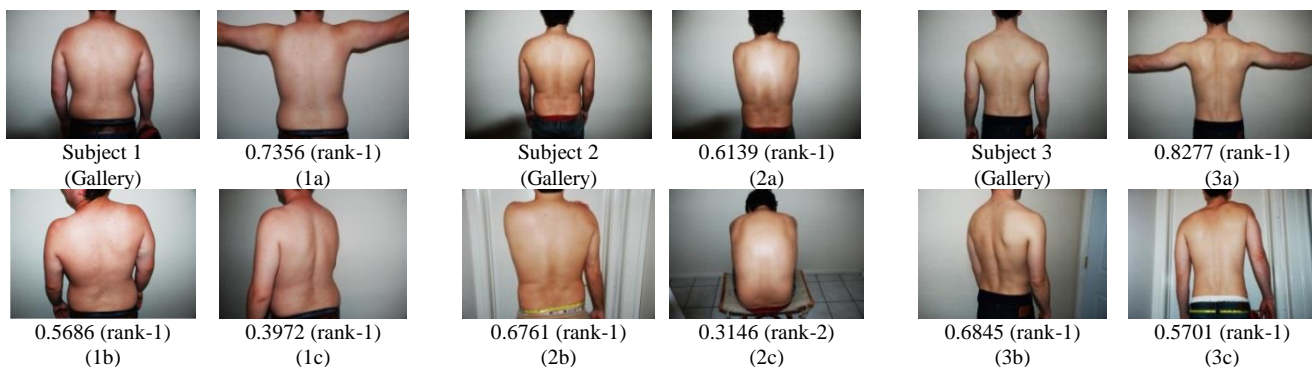


Figure 18. Matching results of three Caucasians' backs captured in different poses and viewpoints.

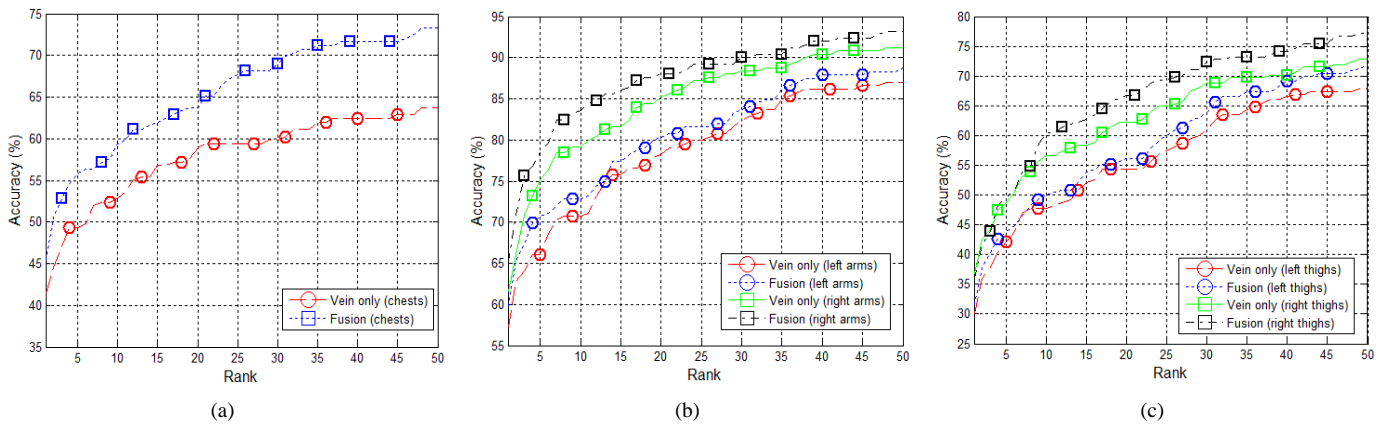


Figure 19. CMC curves of vein identification with and without the fusion with RPPVSM on (a) chests, (b) left and right forearms, and (c) left and right thighs.

our system deals with evidence images, which are always in the form of RGB images only, a vein uncovering method needs to be first applied to the input RGB images to visualize vein patterns, which are previously unclear in the RGB color space. After this process, the vein patterns are extracted and matched with other vein patterns. In this case, the quality of the visualized vein patterns, which actually depends on the acquisition conditions and the quality of the input image itself, will affect the quality of the extracted vein patterns and eventually the matching result. It should be highlighted that near infrared penetrates skin deeper than visible light and therefore, veins in infrared images are clear. Third, users of commercial systems are always cooperative with the systems. However, it is not true for our case because our target users are criminals and victims.

VII. CONCLUSION

While it is rare to observe the criminals' faces in the evidence images of child sexual abuse, masked gunmen, and riots, their non-facial body parts are often visible. To identify the criminals in these skin images, an automated RPPVSM identification system, which is comprised of skin segmentation, RPPVSM detection, and RPPVSM matching algorithms, is proposed in this paper. The RPPVSM identification system was evaluated on 1,200 back images of Asian and Caucasian subjects and the results show that our RPPVSM detection algorithm produces more stable skin mark patterns for identification than the other skin mark detection methods, indicating its potential use in the search for suspects during forensic investigation. However, the performance of RPPVSM identification is affected by the number of RPPVSM available for matching. To handle identification with only a small number of RPPVSM, a fusion scheme combining RPPVSM with vein patterns is also proposed. The fusion scheme adopts an existing vein identification system which visualizes vein patterns in color images by mapping RGB values to NIR intensity values. The fusion was evaluated on 2,360 images of chests, forearms, and thighs of mostly Asian subjects. Experimental results show that the fusion improves vein identification in all body parts with improvement rates

varying between 2% to 5% depending on the number of RPPVSM in the skin. According to our best knowledge, this work is the first systematic study on non-facial skin marks and their fusion with vein patterns for automated personal identification in forensic settings. A database will be publicly available by March of 2015 for research purposes.

ACKNOWLEDGMENT

We would like to thank Dr. Noah Craft for providing constructive comments on the preliminary version of this work. This work is partially supported by the Ministry of Education, Singapore through Academic Research Fund Tier 2 MOE2012-T2-1-024.

REFERENCES

- [1] "London Riots: The Third Night – Monday 8 August 2011," *The Guardian* Aug. 8, 2011 [Online]. Available: <http://www.guardian.co.uk/uk/blog/2011/aug/08/london-riots-third-night-live>
- [2] "Athens Reduced to Smoldering Battlefield – in Pictures," *Roarmag* Jun. 30, 2011 [Online]. Available: <http://roarmag.org/2011/06/pictures-athens-austerity-vote-protests-riot/>
- [3] "Lebanon Aghast as Return of Sectarian Kidnappings Raises Spectre of Civil War," *The Guardian* Aug. 15, 2012 [Online]. Available: <http://www.guardian.co.uk/world/2012/aug/15/lebanon-syria-sectarian-kidnappings-warnings>
- [4] "Occupy Protest in Rome Hijacked by Rioters who Cause Damage Put at Euro 2m," *The Guardian* Oct. 16, 2011 [Online]. Available: <http://www.guardian.co.uk/world/2011/oct/16/rome-riot-damage-ringleaders-police>
- [5] "Inflation Rises and Chaotic Public Services Led Us Here," *ITV* Jun. 25, 2013 [Online]. Available: <http://www.itv.com/news/2013-06-19/inflation-rises-and-chaotic-public-services-led-us-here/>
- [6] A. Nurhudatiana, A. W.-K. Kong, K. Matinpour, S.-Y. Cho, and N. Craft, "Fundamental Statistics of Relatively Permanent Pigmented or Vascular Skin Marks for Criminal and Victim Identification," in *Proc. IJCB*, pp. 1-6, 2011.
- [7] A. Nurhudatiana, A.W.-K. Kong, K. Matinpour, D. Chon, L. Altieri, S.Y. Cho, and N. Craft, "The Individuality of Relatively Permanent Pigmented or Vascular Skin Marks (RPPVSM) in Independently and Uniformly Distributed Patterns," *IEEE TIFS*, vol. 8, no. 6, pp. 998-1012, 2013.
- [8] The U.S. Attorney's Office, Central District of California, Release No. 08-074, "Ex-marine Guilty of Using Drugs and Force to Have Sex with

- Young Girls in Cambodia,” 29 May 2008. Available: <http://www.justice.gov/usao/cac/Pressroom/pr2008/074.html>
- [9] United States v. Pepe, Case No. 07-168-DSF. Trial transcript, May 5, 2008.
- [10] J.M. Grichnik, A.R. Rhodes, and A.J. Sober, *Fitzpatrick's Dermatology in General Medicine*, 7th ed., McGraw-Hill, 2008.
- [11] W. James, T. Berger, and D. Elston, *Andrew's Diseases of the Skin: Clinical Dermatology*, 10th ed., Saunders, 2005.
- [12] D. Lin and X. Tang, “Recognize High Resolution Faces: From Macrococosm to Micrococosm,” in *Proc. IEEE CVPR*, pp. 1355-1362, 2006.
- [13] J.S. Pierrard and T. Vetter, “Skin Detail Analysis for Face Recognition,” in *Proc. CVPR*, pp. 1-8, 2007.
- [14] Z. Zhang, S. Tulyakov, and V. Govindaraju, “Combining Facial Skin Mark and Eigenfaces for Face Recognition,” in *Proc. ICB*, pp. 424-433, 2009.
- [15] U. Park and A.K. Jain, “Face Matching and Retrieval Using Soft Biometrics,” *IEEE TIFS*, vol. 5, no. 3, pp. 406-415, 2010.
- [16] N. Srinivas, G. Aggarwal, P.J. Flynn, and R.W.V. Bruegge, “Analysis of Facial Marks to Distinguish Between Identical Twins,” *IEEE TIFS*, vol. 7, no. 5, pp. 1536-1550, 2012.
- [17] D.G. Lowe, “Distinctive Image Features from Scale Invariant Keypoints,” *IJCV*, vol. 60, no. 2, pp. 91-110, 2004.
- [18] P.F. Felzenszwalb and D.P. Huttenlocher, “Pictorial Structures for Object Recognition,” *IJCV*, vol. 61, no. 1, pp. 55-79, 2005.
- [19] V. Blanz and T. Vetter, “A Morphable Model for the Synthesis of 3D Faces,” in *SIGGRAPH '99 Proc. 26th Annual Conf. Computer Graphics and Interactive Techniques*, pp. 187-194, Los Angeles, 1999.
- [20] T.F. Cootes, G.J. Edwards, and C.J. Taylor, “Active Appearance Models,” in *Proc. ECCV*, vol. 2, pp. 484-498, 1998.
- [21] D. Ziou and S. Tabbone, “Edge Detection Techniques: An Overview,” *IJPRAI*, vol. 8, no. 4, pp. 537-559, 1998.
- [22] A.K. Jain, K. Nandakumar, and A. Ross, “Score Normalization in Multimodal Biometric Systems,” *Pattern Recognition*, vol. 38, no. 12, pp. 2270-2285, 2005.
- [23] T.F. Cootes, C.J. Taylor, D.H. Cooper, and J. Graham, “Active Shape Models-Their Training and Application,” *Computer Vision and Image Understanding*, vol. 61, no. 1, pp. 38-59, 1995.
- [24] G. Loy and A. Zelinsky, “Fast Radial Symmetry for Detecting Points of Interest,” *IEEE TPAMI*, vol. 25, no. 8, pp. 959-973, 2003.
- [25] P. Burt and E. Adelson, “The Laplacian Pyramid as a Compact Image Code,” *IEEE Trans. Communication*, vol. 31, no. 4, pp. 532-540, 1983.
- [26] C. Bradley, *The Algebra of Geometry: Cartesian, Areal and Projective Co-Ordinates*, Bath: Highperception, 2007.
- [27] S. Milborrow and F. Nicolls, “Locating Facial Features with an Extended Active Shape Model,” in *Proc. ECCV*, pp. 504-513, 2008.
- [28] R. Friedman, D. Rigel, and A. Kopf, “Early Detection of Malignant Melanoma: The Role of Physician Examination and Self-Examination of the Skin,” *CA: A Cancer Journal for Clinicians*, vol. 35, no. 3, pp. 130-151, 1985.
- [29] T.S. Cho, W.T. Freeman, and H. Tsao, “A Reliable Skin Mole Localization Scheme,” in *Proc. ICCV*, pp. 1-8, 2007.
- [30] T.K. Lee, M.S. Atkins, M.A. King, S. Lau, and D.I. McLean, “Counting Moles Automatically From Back Images,” *IEEE Trans. Biomedical Engineering*, vol. 52, no. 11, pp. 1966-1969, 2005.
- [31] D. Comanicu and P. Meer, “Mean Shift: A Robust Approach Toward Feature Space Analysis,” *IEEE TPAMI*, vol. 24, no. 5, pp. 603-618, 2002.
- [32] D. Perednia and R. White, “Automatic Registration of Multiple Skin Lesions by Use of Point Pattern Matching,” *Computerized Medical Imaging and Graphics*, vol. 16, no. 3, pp. 205-216, 1992.
- [33] R.G. White and D.A. Perednia, “Automatic Derivation of Initial Match Points for Paired Digital Images of Skin,” *Computerized Medical Imaging and Graphics*, vol. 16, no. 3, pp. 217-225, 1992.
- [34] J. Roning and M. Riech, “Registration of Nevi in Successive Skin Images for Early Detection of Melanoma,” in *Proc. ICPR*, pp. 352-357, 1998.
- [35] B. McGregor, “Automatic Registration of Images of Pigmented Skin Lesions,” *Pattern Recognition*, vol. 31, no. 6, pp. 805-817, 1998.
- [36] H. Huang and P. Bergstresser, “A New Hybrid Technique for Dermatological Image Registration,” in *Proc. IEEE Int. Conf. Bioinformatics and Bioengineering*, pp. 1163-1167, 2007.
- [37] H. Mirzaalian, G. Hamarneh, and T. Lee, “A Graph-Based Approach to Skin Mole Matching Incorporating Template-Normalized Coordinates,” in *Proc. CVPR*, pp. 2152-2159, 2009.
- [38] A. Nurhudatiana, A.W.K. Kong, L. Altieri, and N. Craft, “Automated Identification of Relatively Permanent Pigmented or Vascular Skin Marks (RPPVSM),” in *Proc. ICASSP*, pp. 2984-2988, 2013.
- [39] M. Jones and J. Rehg, “Statistical Color Models With Application to Skin Detection,” *IJCV*, vol. 46, no. 1, pp. 81-96, 2002.
- [40] V. Vezhnevets, V. Sazonov, and A. Andreeva, “A Survey on Pixel-Based Skin Color Detection Techniques,” in *Proc. Graphicon*, pp. 85-92, 2003.
- [41] P. Kakumanu, S. Makrogiannis, and N. Bourbakis, “A Survey of Skin-Color Modeling and Detection Methods,” *Pattern Recognition*, vol. 40, no. 3, pp. 1106-1122, 2007.
- [42] H.D. Cheng, X.H. Jiang, Y. Sun, and J. Wang, “Color Image Segmentation: Advances and Prospects,” *Pattern Recognition*, vol. 34, no. 12, pp. 2259-2281, 2001.
- [43] N.R. Pal and S.K. Pal, “A Review on Image Segmentation Techniques,” *Pattern Recognition*, vol. 26, no. 9, pp. 1277-1294, 1993.
- [44] R.M. Haralick and L.G. Shapiro, “Image Segmentation Techniques,” *Computer Vision, Graphics, and Image Processing*, vol. 29, no. 1, pp. 100-132, 1985.
- [45] J.C. Bezdek, *Pattern Recognition with Fuzzy Objective Function Algorithms*, New York: Plenum Press, 1981.
- [46] V. Madisetti and D.B. Williams, *Digital Signal Processing Handbook*, CRC Press, 1997.
- [47] T. Ojala, M. Pietikäinen, and T. Mäenpää, “Gray Scale and Rotation Invariant Texture Classification with Local Binary Patterns,” in *Proc. ECCV*, pp. 404-420, 2000.
- [48] L. Breiman, J. Friedman, C.J. Stone, and R.A. Olshen, *Classification and Regression Trees*, Chapman & Hall / CRC Press: 1984.
- [49] X.C. He and N.H.C. Yung, “Curvature Scale Space Corner Detector with Adaptive Threshold and Dynamic Region of Support,” in *Proc. ICPR*, vol. 2, pp. 791-794, 2004.
- [50] L.G. Roberts, “Machine Perception of Three-Dimensional Solids,” in *Optical and Electro-Optical Information Processing* (J. Tippett, D. Berkowitz, L. Clapp, C. Koester, A. Vanderburgh, Eds.), MIT Press, pp. 149-197, 1965.
- [51] A. Myronenko and X. Song, “Point Set Registration: Coherent Point Drift,” *IEEE TPAMI*, vol. 32, no.12, pp. 2262-2275, 2010
- [52] C. Tang, A.W.K. Kong, and N. Craft, “Uncovering Vein Patterns from Color Skin Images for Forensic Analysis,” in *Proc. CVPR*, pp. 665-672, 2011.
- [53] H. Zhang, C. Tang, A. Kong, and N. Craft, “Matching Vein Patterns from Color Images for Forensic Investigation,” in *Proc. BTAS*, pp. 77-84, 2012.
- [54] H.R. Sharifzadeh, H. Zhang, and A.W.K. Kong, “Vein Pattern Visualization through Multiple Mapping Models and Local Parameter Estimation for Forensic Investigation,” in *Proc. ICPR*, 2014 (to appear).
- [55] G. Loy and A. Zelinsky, “Fast Radial Symmetry for Detecting Points of Interest,” *IEEE TPAMI*, vol. 25, no. 8, pp. 959-973, 2003.

- [56] H. Su and A.W.K. Kong, "A Study on Low Resolution Androgenic Hair Patterns for Criminal and Victim Identification", *IEEE TIFS*, vol. 9, no. 4, pp. 666-680, 2014.
- [57] A.K. Jain, S. Prabhakar, L. Hong, and S. Pankanti, "Filterbank-Based Fingerprint Matching," *IEEE TIP*, vol. 9, no. 5, pp. 846-859, 2002.
- [58] L. Wang, G. Leedham, and S.-Y. Cho, "Minutiae Feature Analysis for Infrared Hand Vein Pattern Biometrics," *Pattern Recognition*, vol. 41, no. 3, pp. 920-929, 2008.
- [59] N. Miura, A. Nagasaka, and T. Miyatake, "Feature Extraction of Finger-Vein Patterns Based On Repeated Line Tracking and Its Application to Personal Identification," *Machine Vision and Applications*, vol. 15, pp. 194-203, 2004.
- [60] S. Gielen, G. Schuler, and V. Adams, "Cardiovascular Effects of Exercise Training: Molecular Mechanisms," *Circulation*, vol. 122, pp. 1221-1238, 2010.
- [61] H. Zhang, "Blood Vessel Pattern Matching," *Vein Identification for Forensic Investigation*, PhD thesis, Nanyang Technological University, Singapore, 2014 (submitted).
- [62] C. Tang, H. Zhang, A.W.K. Kong, and N. Craft, "Visualizing Vein Patterns from Color Skin Images Based On Image Mapping for Forensic Analysis," in *Proc. ICPR*, pp. 2387-2390, 2012.
- [63] X. Li and A.W.K. Kong, "Restoring Blood Vessel Patterns From JPEG Compressed Skin Images for Forensic Analysis," in *Proc. WIFS*, pp. 19-24, 2013.